SLAC – PUB – 4255
March 1987
(E/I)

DRIFT CHAMBER VERTEX DETECTORS FOR SLC/LEP*

KENNETH G. HAYES

Stanford Linear Accelerator Center
Stanford University, Stanford, California 94305

Presented at the International Conference on Advances
in Experimental Methods for Colliding Beam Physics
Stanford Linear Accelerator Center
Stanford, California
March 9 – 13, 1987

* This work was supported in part by the Department of Energy, contract DE-AC03-76SF00515 (SLAC).

1. INTRODUCTION

The short but measurable lifetimes of the b and c quarks and the tau lepton have motivated the development of high precision tracking detectors capable of providing information on the decay vertex topology of events containing these particles. The significant physics potential of vertex detectors for the study of Z^o decays is widely recognized, and they have been included in the design of all six LEP and SLC experiments. The ALEPH, DELPHI, and SLD experiments will have silicon vertex detectors,[1] while L3 and OPAL will rely on drift chamber vertex detectors. The MARK II experiment will begin data taking with a vertex drift chamber, but will add a silicon strip detector after the first year.[2] In this paper I will review the OPAL, L3, and MARK II vertex drift chambers.

A useful vertex detector for studying Z^o decays must accurately measure track impact parameters within a dense jet environment. Three detector properties are most important: the limiting impact parameter resolution for high momentum tracks (σ_o), the contribution to the impact parameter resolution from multiple Coulomb scattering in the detector and upstream material (σ_{ms}/P where P is the track momentum), and the double track resolution.

To illustrate the requirements on impact parameter resolution, consider the task of tagging B meson decay tracks in $Z \rightarrow b\bar{b}$ events by testing their consistency with originating in the primary event vertex. A track is defined to be tagged if its projected impact parameter (δ) to the event primary vertex (in the XY plane perpendicular to the beam axis) is larger than 3 times the impact parameter error (σ_δ). Figure 1 shows the fraction of tagged B meson decay tracks as a function of the limiting impact parameter resolution, σ_o, for four values of σ_{ms}. For simplicity, it is assumed that the two terms add in quadrature:

$$\sigma_\delta^2 = \sigma_o^2 + \sigma_{ms}^2/P^2 \ . \tag{1}$$

The track tagging efficiency and the rate of change of the tagging efficiency both increase as the impact parameter resolution improves. Therefore it is desirable

to have the highest resolution possible. However, since the momentum of most tracks is below 3 GeV/c, little is gained by making σ_o much less than $\sigma_{ms}/3$.

The large track density in the jet core imposes stiff requirements on the detector double track resolution. Roughly 10% of tracks in $Z \rightarrow b\bar{b}$ events are within 10 mrad of another track in the XY plane. A double track resolution of 500 (1500) μ for a detector located 5 (15) cm from the interaction point is desirable. Good efficiency also demands large solid angle coverage and a minimum volume where the detector is either insensitive or has poor resolution.

The remainder of this paper is organized as follows: section 2 gives a brief discussion of the factors which determine the design of the three vertex chambers, while sections 3, 4, and 5 are devoted to specific descriptions of the OPAL, L3, and MARK II chambers.

2. DESIGN CONSIDERATIONS

Of the many factors influencing chamber design, their function and compatibility with other detector components in the experiment are the most important. The MARK II vertex chamber is designed only to measure track impact parameters in the XY projection, and is surrounded by a large and completely independent central tracking chamber. The OPAL vertex chamber is enclosed within the pressure vessel of the central jet chamber, and must also measure the track coordinates along the beam direction. The L3 vertex detector is the central tracking chamber and performs many functions besides impact parameter measurement.[3]

The SLC and LEP machine parameters also influence the vertex chamber design. The smaller SLC beam pipe allows the MARK II chamber to have a smaller inner radius. This reduces the multiple scattering and improves the limiting impact parameter resolution. Good solid angle coverage is obtained with a shorter chamber. This improves electrostatic stability and allows the sense wire spacing to be reduced thereby improving the double track resolution and increasing the number of measurements per unit track length. The time

interval between beam crossings and uncertainty in the radiation background also affect the design.

The remainder of this section focuses on four aspects of chamber design: global strategy, chamber gas, signal processing, and cell design.

2.1 Global Strategy

The vertex chambers for all three experiments are based on the jet cell geometry. To maximize the impact parameter resolution, the chambers make many measurements on each track and operate at elevated pressures to improve the spatial resolution of each measurement. The limiting impact parameter resolution, σ_o, for a set of N equally spaced measurements which span the radial interval from r_1 to r_2 is given by

$$\sigma_o^2 = \sigma_w^2/N \cdot [1 + 3 \cdot (N-1)/(N+1) \cdot (r_2 + r_1/r_2 - r_1)^2] \qquad (2)$$

where σ_w is the spatial resolution of each measurement. The best resolution is obtained by minimizing r_1, and in the limit where $r_1 = 0$ and $N >> 1$, Eq. 2 becomes

$$\sigma_o = 2 \cdot \sigma_w/\sqrt{N}. \qquad (3)$$

In exploiting the $1/\sqrt{N}$ factor to improve impact parameter resolution, care must be taken to control systematic errors. For example, placement tolerances are more restrictive for the sense wire plane than for individual sense wires. Use of additional tracking information from downstream chambers can improve the impact parameter resolution provided systematic errors are understood.

Chamber segmentation design affects performance in many ways. More segmentation decreases the maximum drift distance and track angle to the anode plane, lowers the voltages on wires used to generate drift fields, and reduces the average wire hit multiplicity. However, it increases the fraction of tracks which pass near anode or cathode wires where the resolution is degraded, and increases

the number of wires. This makes the chamber more complex and worsens the multiple scattering.

The design can be influenced by the need to match segmentation of other detector components, to solve the left-right ambiguity problem, or to allow Z^o coordinate determination using stereo cells or charge division.

2.2 Chamber Gas

Chamber design and performance is affected by the choice of gas. All three groups have conducted prototype studies using a mixture of CO_2 with a small fraction of isobutane.[4] [5] [6] For typical drift fields ($\leq$ 1.5 kV/cm/bar) this gas is "slow" and has a drift velocity which varies linearly with electric field of about 7.5 (μm/nsec)/(kV/cm/bar). For these fields, electron diffusion is near the minimum value determined by the gas temperature. Prototype chamber results for the spatial resolution are shown in Fig. 2. Although the three groups have used different operating points, cell geometries, isobutane concentrations, and time digitization schemes, the conclusion is clear: the spatial resolution varies with drift distance from about 20 to 50 μm for the distances of interest here.

Besides excellent intrinsic resolution, use of slow gases greatly relaxes the requirements on the readout electronics. For a drift velocity of 50 μm/nsec typical of "fast" gases, hits from tracks separated by 500 μm are only 10 nsec apart. Use of slow gases reduces the electronic contribution to both the spatial resolution and the double hit resolution in proportion to the drift velocity, *i.e.* by roughly an order of magnitude. This allows exploitation of available 100 MHz waveform digitizers to significantly improve chamber performance (see section 2.3).

The linear dependence of the drift velocity on the ratio of the electric drift field to the gas density demands the gas properties (pressure, temperature, and composition) and electric field be precisely controlled or monitored to ensure that the drift velocity is known. To simplify the determination of the drift time-to-distance relationship, the drift field should be uniform and stable. This forces

tight tolerances on cathode wire plane location and voltage accuracy. Time variation in the drift field (from charge build-up on dielectric surfaces or from voltage sag in cathode resistor chains due to large chamber currents) must be minimized. Chamber segmentation which minimizes non-uniformity in the drift field is desirable. Although it is difficult to control the absolute chamber temperature, it is important that the gas temperature be uniform. Changes in temperature with time can be monitored and used to either adjust the gas pressure to maintain constant drift velocity or to correct the time-to-distance relationship.

To illustrate the level of control or monitoring required, consider the MARK II chamber (section 5) which has a limiting impact parameter resolution of about 20 μm (Eq. 2). Assuming the systematic error in the impact parameter due to uncertainty in the drift velocity should be no larger than 25% of the statistical error, the drift velocity must be known to an accuracy of .025% for a typical drift distance of 2 cm. The electric drift field and the gas temperature and pressure must be stable or monitored to this accuracy. For isobutane concentrations between 5 and 20%, the fractional change in drift velocity is about 1% for a 1% increase in the isobutane concentration. Thus the isobutane fraction in the gas must be maintained to an accuracy of .00025.

Another disadvantage of slow and cool gases is the higher fields required on the sense wires for gain. This worsens the sense wire stability tension requirements, increases the stored energy in the field, and increases the surface fields on nearby wires. The linear dependence of the drift velocity on electric field degrades cell isochrony since ionization electrons which drift to the sense wire near the edge of a cell not only travel longer distances to reach the wire (see Fig. 5), but also traverse low field regions.

As a possible alternative to slow gases, the OPAL and MARK II groups have both made prototype measurements with the "fast" 50/50 mixture of argon/ethane. For fields between .75 and 1.5 kV/cm/bar, the drift velocity varies slowly between 50 and 52 μm/nsec. Figure 3 shows the prototype results for the

spatial resolution as a function of drift distance. To achieve maximum spatial resolution with currently available electronics, threshold timing must be used (see section 2.3) and this limits the attainable double track resolution. It is clear that although the slow, cool gases are difficult to use, they provide considerably improved performance.

2.3 Signal Processing

Large track densities in the jet core demand excellent multi-hit capability in the readout electronics. For slow gases, readout electronics based on inexpensive 100 MHz 6 bit flash-ADCs have several advantages over discriminator/TDC timing. The pattern recognition ability of the waveform sampling method allows closely-spaced or overlapping hits to be separated, and clearly distinguished from late arriving clusters from the preceding hit. Mark II prototype results on the second hit detection efficiency as a function of separation are shown in Fig. 4.

For drift distance exceeding a few mm in the CO_2 mixtures, the sampling method gives a modest improvement in the spatial resolution. In Mark II prototype studies comparing FADC and TDC results, the contribution to the spatial resolution from electron diffusion in the drift region was reduced by about 10 to 20%.

Both the spatial and the double track resolutions for a 100 MHz FADC readout system deteriorate as the drift velocity increase. Degradation occurs for hits within about 1 mm of the sense wires in slow gases. The 10 nsec sampling interval is too long for the intrinsic spatial resolution of fast gases to be realized, and TDC methods give superior results. The double track resolution of fast gas TDC systems has been limited to about 2 mm due to the difficulty of building analog shaping electronics and multihit TDCs which can measure closely-spaced hits to the required accuracy.

2.4 Cell Design

The design of the cell amplification region (where the uniform drift field transforms into the $1/r$ field near the sense wire) influences all aspects of chamber

performance, but particularly affects the sense wire electrostatic stability and the double track capability. The designs for the OPAL, Mark II, and L3 detectors are illustrated in Fig. 5 which shows the electron drift trajectories in the amplification region for optimized wire charge configurations.

The anode plane in the OPAL chamber, Fig. 5a, contains alternating sense and potential wires. For a fixed drift field, the potential wire charge is selected to give the appropriate sense wire surface field required for gain. For tracks at small angles to the sense plane, the contribution to the double track resolution from the cell charge collection geometry is of order 1/2 the sense wire spacing. The minimum sense wire spacing is set by the electrostatic stability requirements at the desired operating point.

Two grid planes surround the anode plane in the Mark II design (Fig. 5b) and provide an additional degree of freedom in setting the wire charge configuration. This freedom is used to optimize the sense wire stability and to improve cell isochrony by focusing the drift trajectories. Improved stability allows the sense wire spacing to be decreased benefiting both the double track resolution and the hit measurement density.

The L3 time expansion chamber, conceptually illustrated in Fig. 5c, incorporates two unique concepts. A fine wire mesh (simulated in Fig. 5c by closely-spaced wires) cleanly separates the uniform drift region from the "detection gap." The mesh wire spacing is small enough that transit time differences through the mesh are insignificant. The electric field on the sense wire side is decoupled from the drift region electric field, and can be adjusted so that both potential and sense wire charges are positive. The length of the track ionization segment which terminates on the sense wire is determined by the ratio of the sense and potential wire charges. For gases whose drift velocity varies linearly with electric field in the drift region, the discontinuous jump in field across the wire mesh affectively increases the cell isochrony since transit time variations for different drift trajectories in the detection gap are reduced.

There are some disadvantages to the TEC design. The need for positively charged potential wires greatly increases the sense wire tension needed for electrostatic stability. A long chamber cannot operate with pressurized slow gases with the field configuration illustrated in Fig. 5c without additional sense wire supports placed periodically along the wire. Although very isochronous chambers perform excellently for tracks parallel to the anode plane, the spatial resolution deteriorates markedly as the track angle increases.

3. THE OPAL VERTEX CHAMBER

The wire configuration of the OPAL vertex chamber is illustrated in Fig. 6. The chamber is 100 cm long, and has 1 axial and 1 stereo layer each containing 36 radial jet cells. The stereo cells are formed by stringing wires between endplate locations rotated by 20^o (2 cells). The axial (stereo) cells have 12 (6) sense wires spaced by 5.0 (5.3) mm with the innermost wire at a radius of 10.3 (18.8) cm. The left-right ambiguity is resolved by staggering alternate wires by ± 41 μm which electrostatic forces increase to about ± 80 μm at the chamber center.

A 1 mm thick carbon fiber tube at the outer radius (232 mm) and an aluminized mylar foil at the inner radius serve to define a separate gas volume within the pressure vessel of the central tracking chamber which operates up to 4 bars pressure. The outer tube also provides the main mechanical support between the two 32 mm thick fiberglass endplates. The beam pipe serves as the pressure vessel inner wall and has a thin central section ($|Z| < 30$ cm) made from a 1.2 mm thick layer of carbon fiber on a .2 mm thick aluminum liner. The pipe is .86% of a radiation length thick, and at a radius of 7.8 cm, contributes about 100 μm$\cdot$(GeV/c) to the impact parameter resolution (σ_{ms}).

Cathode and anode wires are positioned using grooved plexiglas combs that are mounted to the endplates with glass dowels. The location accuracy of the anode comb grooves relative to the dowels is about 5 μm (sigma), and the accuracy of the dowel placement in the endplates is about 6 μm. Feedthroughs in the endplates locate the field shaping wires at the cell inner and outer bound-

aries. Aluminized mylar foils are used to complete the cell closure. Cathode wires are powered using resistor divider chains, and can produce drift fields up to 3.7 kV/cm.

The 648 anode wires are read out at both ends using preamps located on the chamber endplates. The timing electronics consists of constant fraction discriminators and a novel multi-hit TDC system[7] which measures both the mean and the difference of the hit times from each end to give the drift distance and Z coordinate along the wire. Provisions are included to water cool the preamplifier/HV distribution compartments.

Results from a 1986 beam test on a prototype chamber containing 4 axial and 2 stereo cells in the final detector geometry are included in Figs. 2 and 3. The double track resolution is expected to be about 2 mm.

The chamber is nearing completion and is scheduled to be installed at the end of 1987.

4. THE L3 VERTEX CHAMBER

The high performance achieved with slow, cool gases has enabled the L3 group to design a vertex chamber which also serves as the central tracking chamber. The chamber is 1 meter long and 93 cm in diameter (see Fig. 7). It is radially segmented into two layers of jet cells that are based on the TEC principle. The inner (outer) layer is divided into 12 (24) radial cells each containing 8 (62) sense wires spaced by 4.8 mm. The radius of the innermost wire is 91 (153) mm. The chamber is designed to operate at pressures up to 2 bars, and has a Be inner pressure wall at 85 mm radius. The inner wall plus Be beam pipe are .85% of a radiation length thick, and contribute about 110 μm·(GeV/c) to σ_{ms}.

The cell design in the detection gap is illustrated in Fig. 7b. The nickel-coated polyester mesh grid is made from 50 μm diameter threads on a 250 μm pitch, and weighs 30 gms/meter^2. The grid/anode spacing is 3 mm. The left-right ambiguity is resolved by sealing off the grid on one side of 16 selected anode wires in the outer layer. The staggered orientation of the inner and outer layers

also aids ambiguity resolution. Charge division readout on 14 wires in the outer layer is used to measure the track coordinate along the beam axis. Except for the charge division wires which are read out at both ends, the sense wires are read out at one end into a 100 MHz waveform sampler (6 bit TRW 1029-J7C). With the TEC operating point adjusted so that the length of track sampled is 2 mm, the double track resolution is expected to be about 600 μm.

The chamber design is in its final stages, and construction should start by the end of 1987.

5. THE MARK II VERTEX CHAMBER

Besides good spatial resolution and double track capability, a primary design objective of the Mark II vertex chamber was the control of sources of systematic error in the impact parameter. Construction techniques designed to produce mechanically precise and identical cells were developed. Minimal segmentation (1 layer containing 10 jet cells) was selected to reduce complexity and to minimize the fraction of the drift volume with non-uniform field. The use of nonradial cells with a large azimuthal tilt angle provides a means to calibrate the chamber using tracks which cross cell boundaries. The tilt angle also resolves the left-right ambiguity, and ensures that no track will be poorly measured along its entire length.

The chamber, illustrated in Fig. 8, covers the radial interval from 4.5 to 19.0 cm, and nearly fills the volume between the SLC beam pipe and the inner wall of the central tracking chamber. The wires for each of the 10 jet cells are strung between pieces of machinable ceramic (Macor), which are then mounted on the chamber frame. Separate endplates allow pressurized operation up to 3 bars. The beam pipe consists of a .25 mm thick layer of carbon fiber wound on a .10 mm thick aluminum liner and is at a radius of 2.5 cm. The 1.2 mm thick beryllium inner wall and the beam pipe are a total of .61% of a radiation length, and contribute 45 μm·GeV/c to σ_{ms}. The active sense wire length is 55 cm.

Figure 9 illustrates the chamber wire pattern. The anode plane contains 41

potential wires spaced by 2.9 mm, and 40 sense wires placed midway between them. The plane has an azimuthal tilt angle of 15.137^o at the radius of the first potential wire (5.127 cm). Two planes of grid wires are placed 1.8 mm on either side of the potential wires (see Fig. 5b). The cathode planes contain 59 wires spaced by 2.0 mm and bisect the angle between the two adjacent sense planes. Guard wires and copper-clad kapton sheets epoxied to the pressure walls terminate the drift field at the inner and outer radius. Aluminium "wings" are placed between the outer wall and the anode and cathode planes to lower the surface fields on the wires near the cell boundaries. The drift field magnitude in the shaded region of Fig. 9 is uniform to .1%.

Knowledge of sense wire locations and deflections and the generation of a uniform drift field impose strict tolerances on the location accuracy of nearly all chamber wires. Use of individual feedthroughs to locate wires is difficult given the small wire spacing and the required location accuracy. Therefore, a different technique designed to produce precisely located *planes* of wires was developed. Complete wire planes are constructed by winding wire at the proper tension around sets of precisely machined grooved Invar cylinders. The wires are located to an accuracy of a few μm in both coordinates over the full width of the plane. The wire planes are then placed in the correct location *above* the surface of the Macor support pieces, shown in Fig. 10, and are glued into place. Once the glue is set, the wires are soldered to flexible copper-clad kapton printed circuits which are attached to the Macor support pieces, and are then cut away from the winding frame. The machining tolerances on the surface of the Macor pieces are loose (a few mils) since the wires do not touch them.

The Macor pieces are positioned by machining the back surface flat, and locating this surface on the chamber endplates (or assembly jigging during construction) using two stainless steel ball bearings which fit into sockets glued into the Macor and endplates. The precision of this location technique is a few μm. Sockets are epoxied into position in the Macor pieces, the chamber endplates, and assembly jigging using a single gage which defines the socket location. Thus

all similar Macor pieces are interchangeable.

The kapton printed circuits are brought through the pressure walls and are attached via custom-made connectors to circuit boards. At one end of the chamber the cathode and guard wires are connected to resistor chains which supply the high voltage. At the other end, sense wires are connected to preamplifiers which drive 50 ohm coaxial cables. The first and last sense wire in each cell are not instrumented. Readout is provided by 100 MHz 6-bit waveform samplers that have a memory depth of 1024 samples. Filters are used to cancel the $1/t$ positive ion tail. Water channels on the pressure endplates and outer cylinder stabilize the chamber temperature.

The chamber is currently under construction, and installation in the Mark II detector at SLC is scheduled for the fall of 1987.

6. CONCLUSIONS

Vertex detectors will be powerful tools for revealing the physics of Z^o decays at SLC and LEP. Given the low momenta of decay tracks from many of the most interesting processes, multiple Coulomb scattering imposes significant limits on the obtainable impact parameter resolution. The beam pipe diameter sets the scale of the multiple scattering and the chamber dimensions. The minimum sense wire spacing, which is limited by electrostatic stability and scales like the square of the chamber length, determines the maximum hit density and the double track capabilities of the chamber.

Spatial resolution obtained with pressurized slow, cool gases of about 30 μm for drift distances of 1 cm, provide impact parameter resolutions which are well matched to the limits imposed by multiple scattering. Double track resolutions in the range of 500 to 1000 μm will allow impact parameter measurements to be made for tracks within the jet core. Many spatial measurements are used to determine a track impact parameter, and systematic errors are an important concern. Precise control of mechanical tolerances, the drift field, and the gas temperature, pressure, and composition are required.

7. ACKNOWLEDGEMENTS

I would like to thank R. Carnegie and S. Llyod from the OPAL collaboration, and G. Viertel from L3 for providing me the latest information on their vertex chambers.

REFERENCES

1. See the contributions by R. Horisberger and S. Watts in these proceedings.
2. See contribution by A. Litke in these proceedings.
3. The SLD, ALEPH, and DELPHI central tracking chambers also measure track impact parameters, but since these chambers have upstream silicon detectors whose primary function is vertex detection, they are not reviewed here.
4. V. Commichau *et al.*, Nucl. Instr. and Meth. **A235** (1985) 267. See also H. Anderhub *et al.*, Nucl. Instr. and Meth. **A252** (1986) 357.
5. R. Carnegie, OPAL collaboration, private communication.
6. J. Alexander *et al.*, Nucl. Instr. and Meth. **A252** (1986) 350.
7. The OPAL Detector Technical Proposal, CERN/LEPC/83-4

FIGURE CAPTIONS

1. The fraction of B meson decay tracks which have an impact parameter to the primary event vertex larger than 3 times the measurement error verses the limiting impact parameter resolution, σ_o. Curves are shown for 4 values of the multiple Coulomb scattering contribution, σ_{ms} (in μm·GeV/c).

2. Prototype chamber results for the spatial resolution verses drift distance in CO_2/isobutane. The gas pressure and isobutane concentration for the OPAL/L3/MARK II results are 2.5/2.0/3.0 bars and 20/20/8% respectively.

3. Prototype chamber results for the spatial resolution verses drift distance in 3 bars of 50/50 argon/ethane.

4. Efficiency for detecting a second track as a function of the track separation for two different grid configurations in the Mark II prototype chamber.

5. Electron drift trajectories in the amplification region for the a) OPAL, b) Mark II, and c) L3 vertex chambers. The wire mesh grid in the L3 TEC is simulated by a plane of closely-spaced wires.

6. Wire pattern of the OPAL vertex chamber. The lines connecting wires in the stereo layer illustrate how the cells are formed.

7. Wire pattern of the L3 vertex chamber; a) the cell arrangement, b) detail of the detection gaps.

8. Isometric view of the Mark II vertex chamber.

9. Wire pattern of the Mark II vertex chamber. The drift field magnitude in the shaded region is within .1% of the central value.

10. Schematic view of the Macor endpiece, kapton artwork, and pressure feedthrough used to support wire planes in the Mark II vertex chamber.

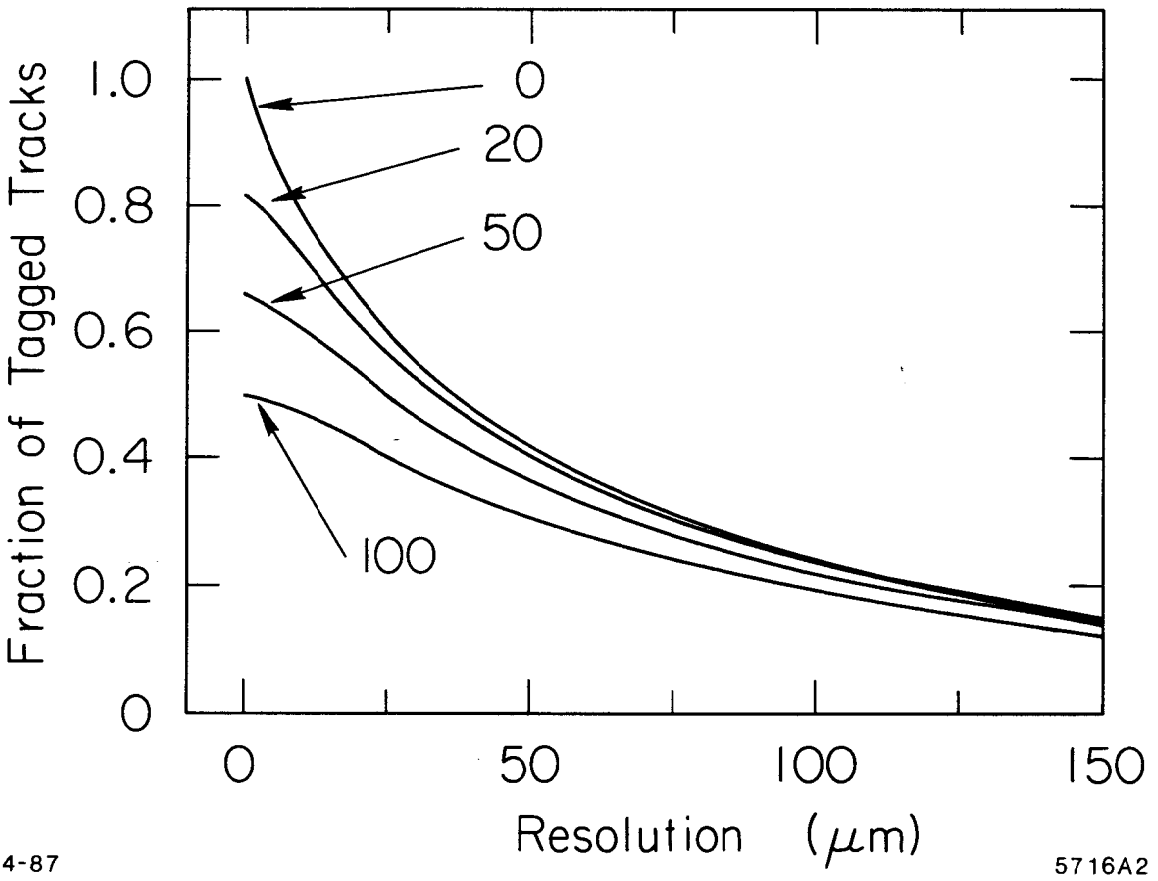
Fraction of Tagged Tracks
1.0
0.8
0.6
0.4
0.2
0
0
50
100
150
Resolution (μm)
0
20
50
100
4-87
5716A2

Fig. 1

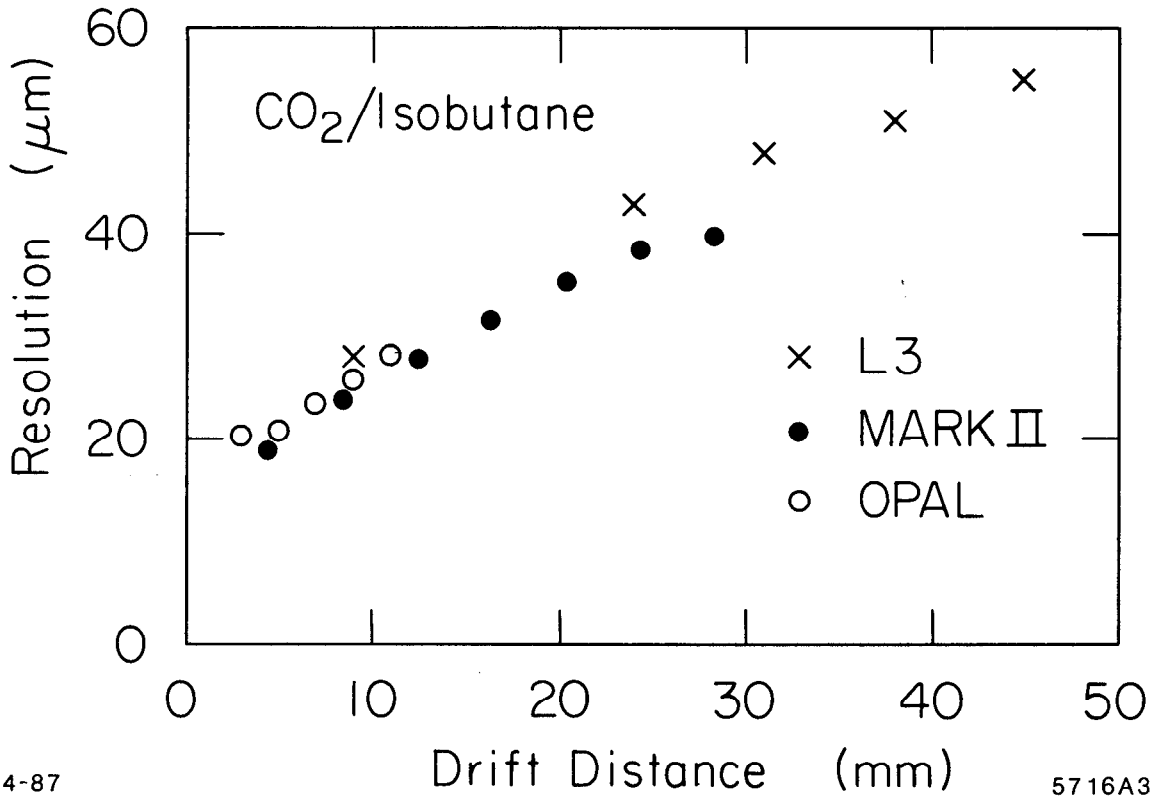
60
40
20
0
Resolution (μm)
CO_2/Isobutane
L3
MARK II
OPAL
0
10
20
30
40
50
Drift Distance (mm)
4-87
5716A3

Fig. 2

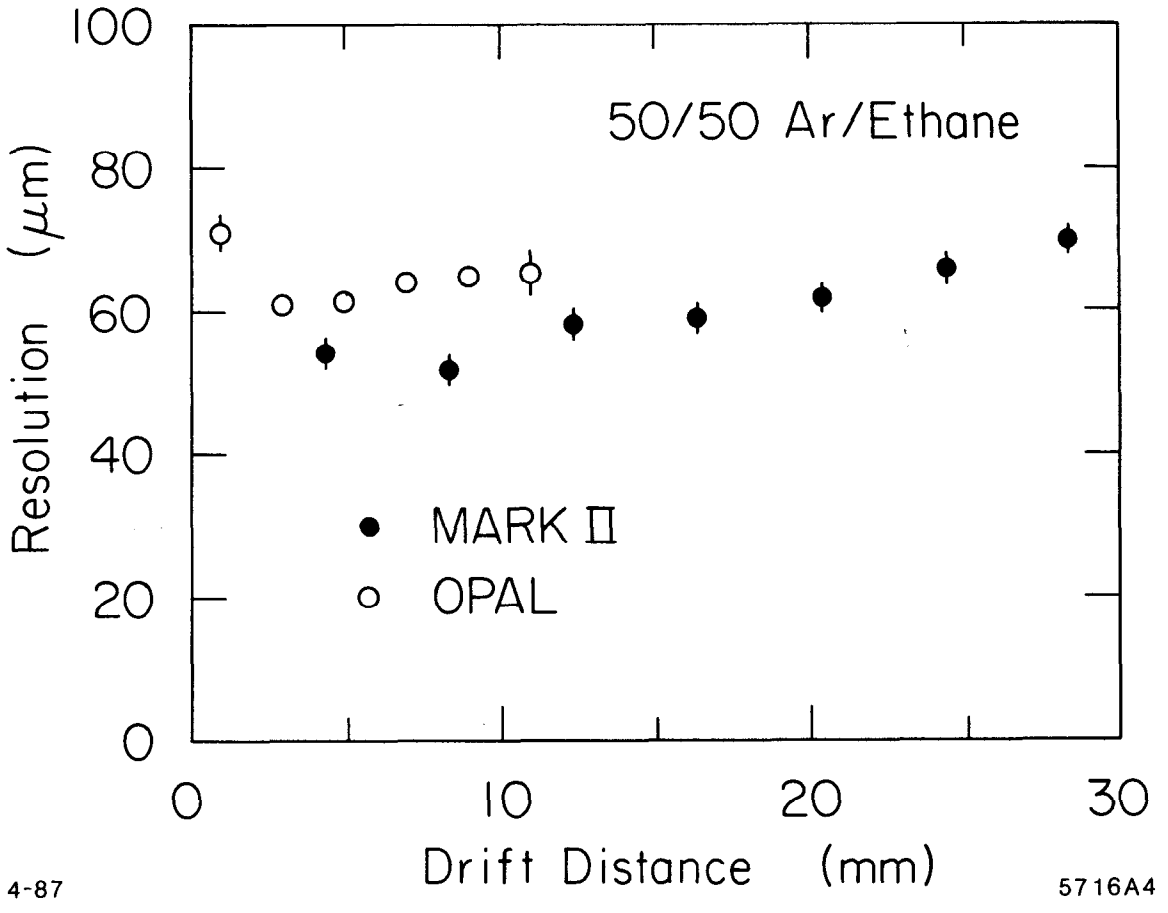
100
80
60
40
20
0
Resolution (μm)
50/50 Ar/Ethane
MARK II
OPAL
0
10
20
30
Drift Distance (mm)
4-87
5716A4

Fig. 3

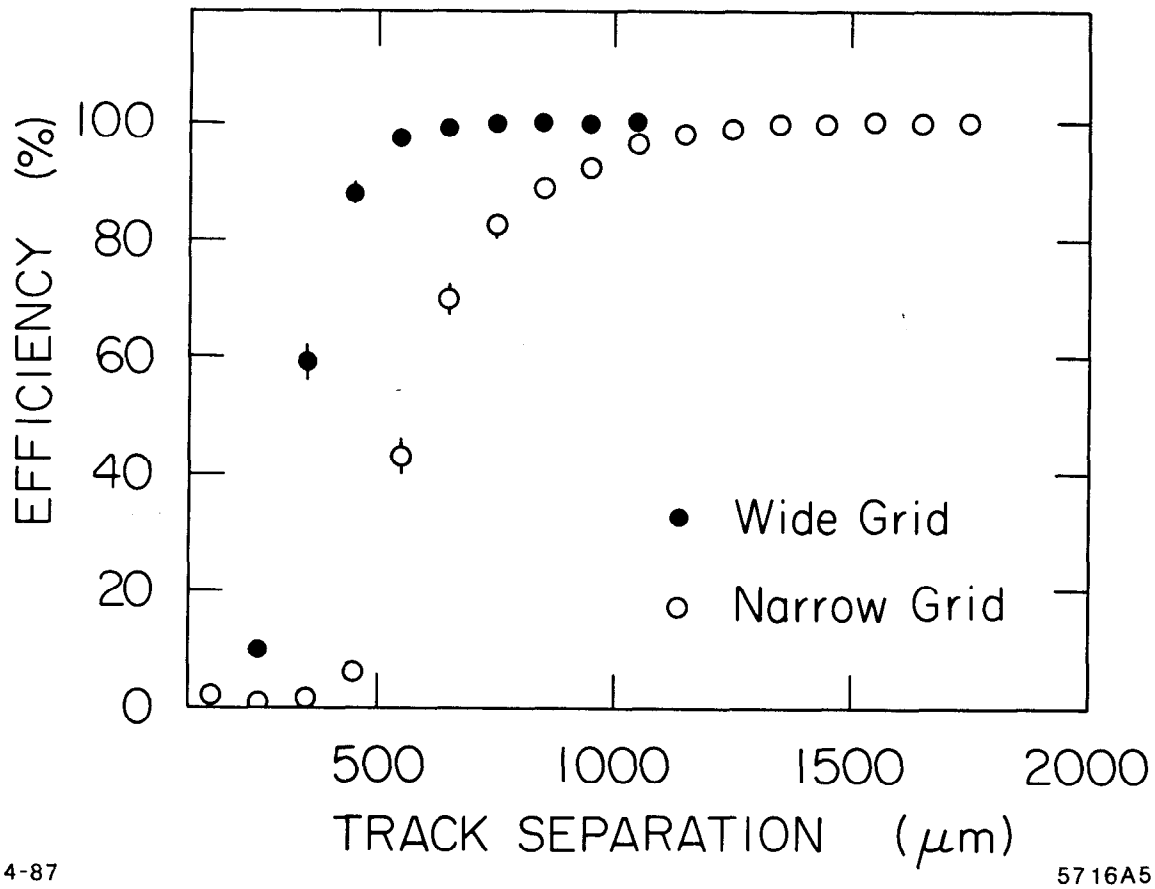
EFFICIENCY (%)
100
80
60
40
20
0
500
1000
1500
2000
TRACK SEPARATION (μm)
Wide Grid
Narrow Grid
4-87
5716A5

Fig. 4

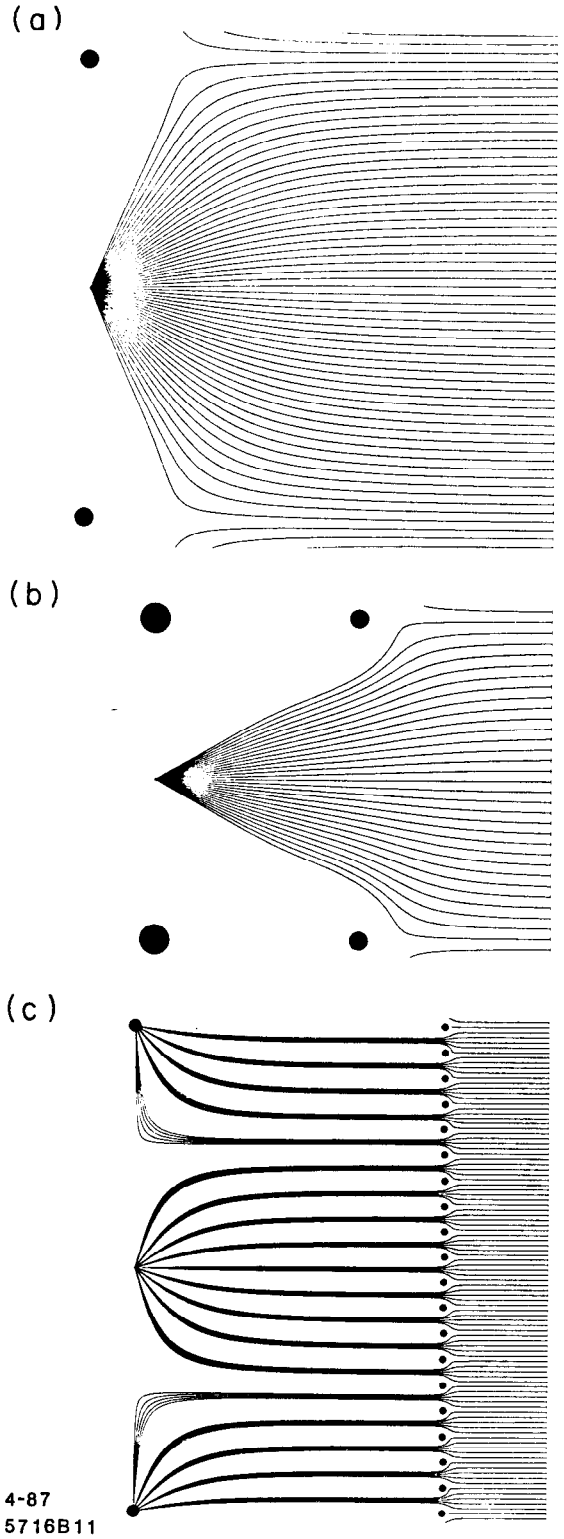

Fig. 5

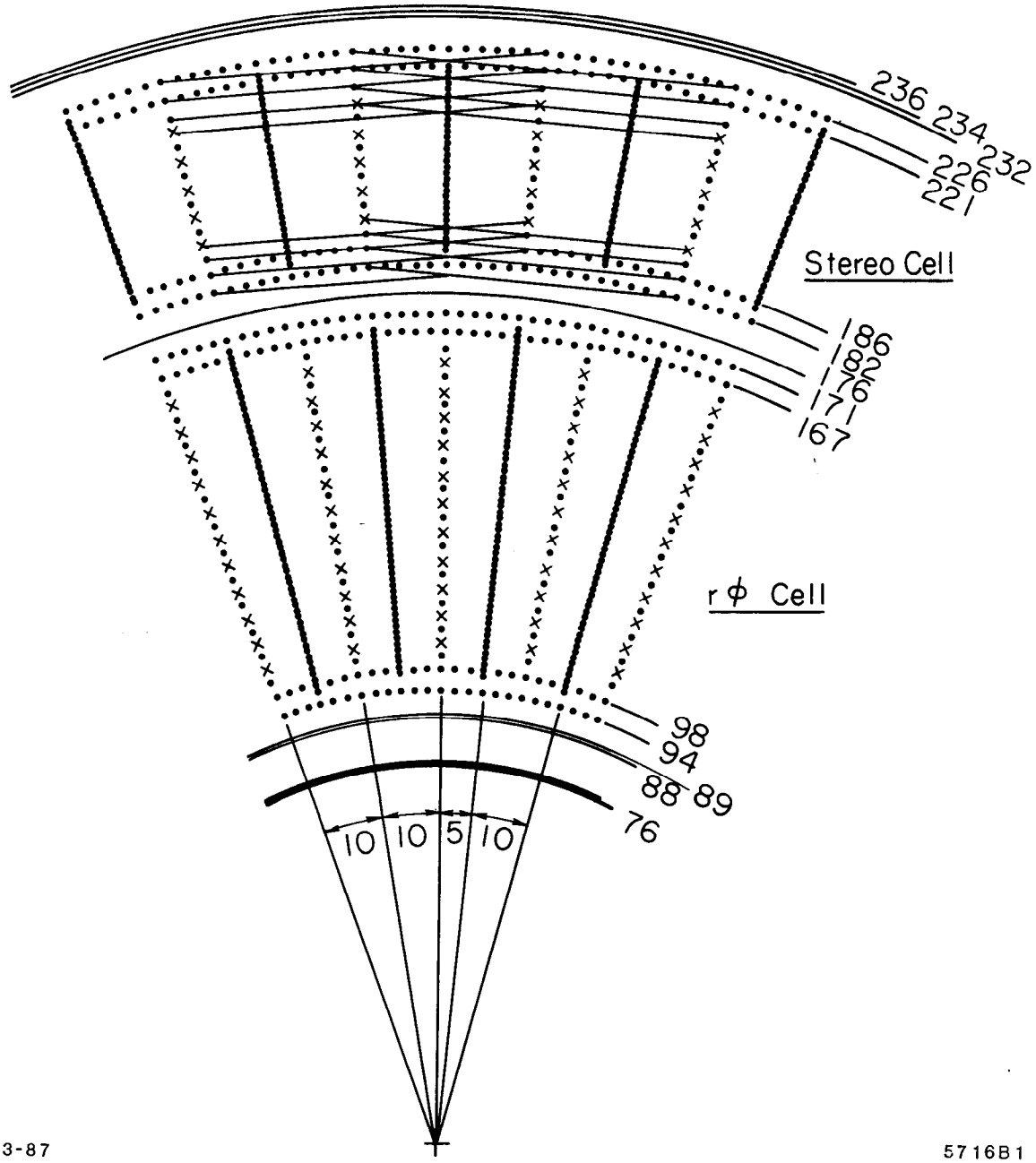
236
234
232
226
221
Stereo Cell
186
182
176
171
167
rφ Cell
98
94
88
89
76
10
10
5
10
3-87
5716B1

Fig. 6

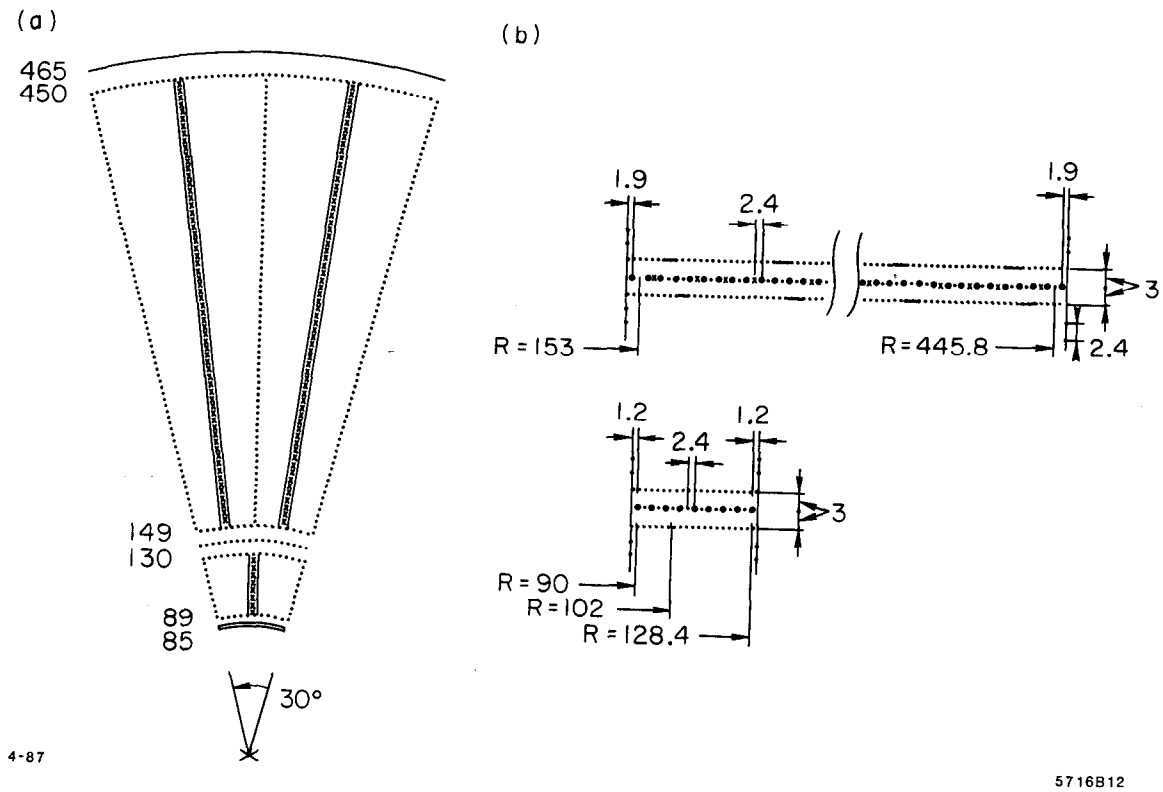
(a)
465
450
149
130
89
85
30°
4-87
(b)
1.9
2.4
1.9
3
R = 153
R = 445.8
2.4
1.2
2.4
1.2
3
R = 90
R = 102
R = 128.4
5716B12

Fig. 7

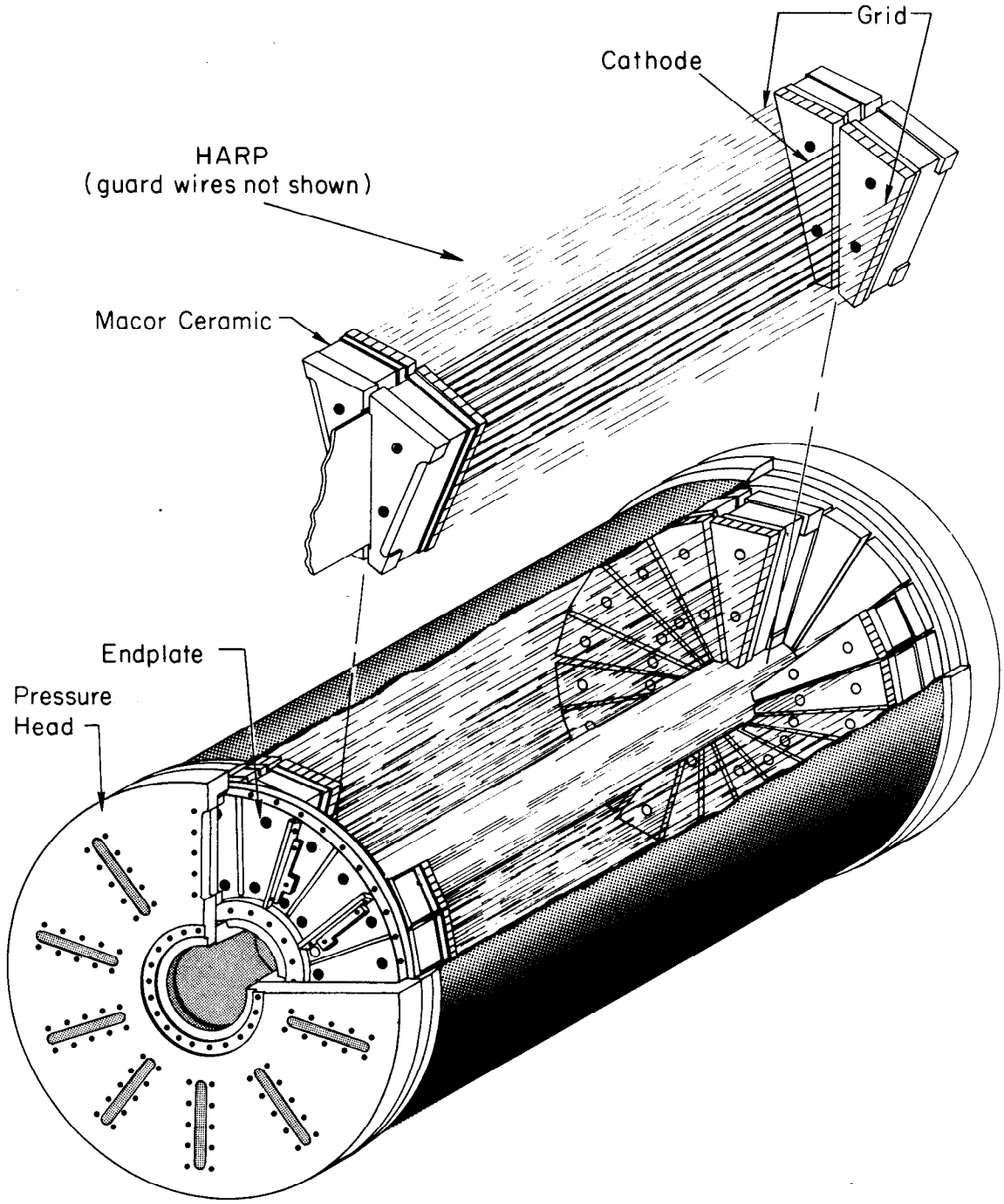

DRIFT CHAMBER VERTEX DETECTOR

7-85

5184B1

Fig. 8

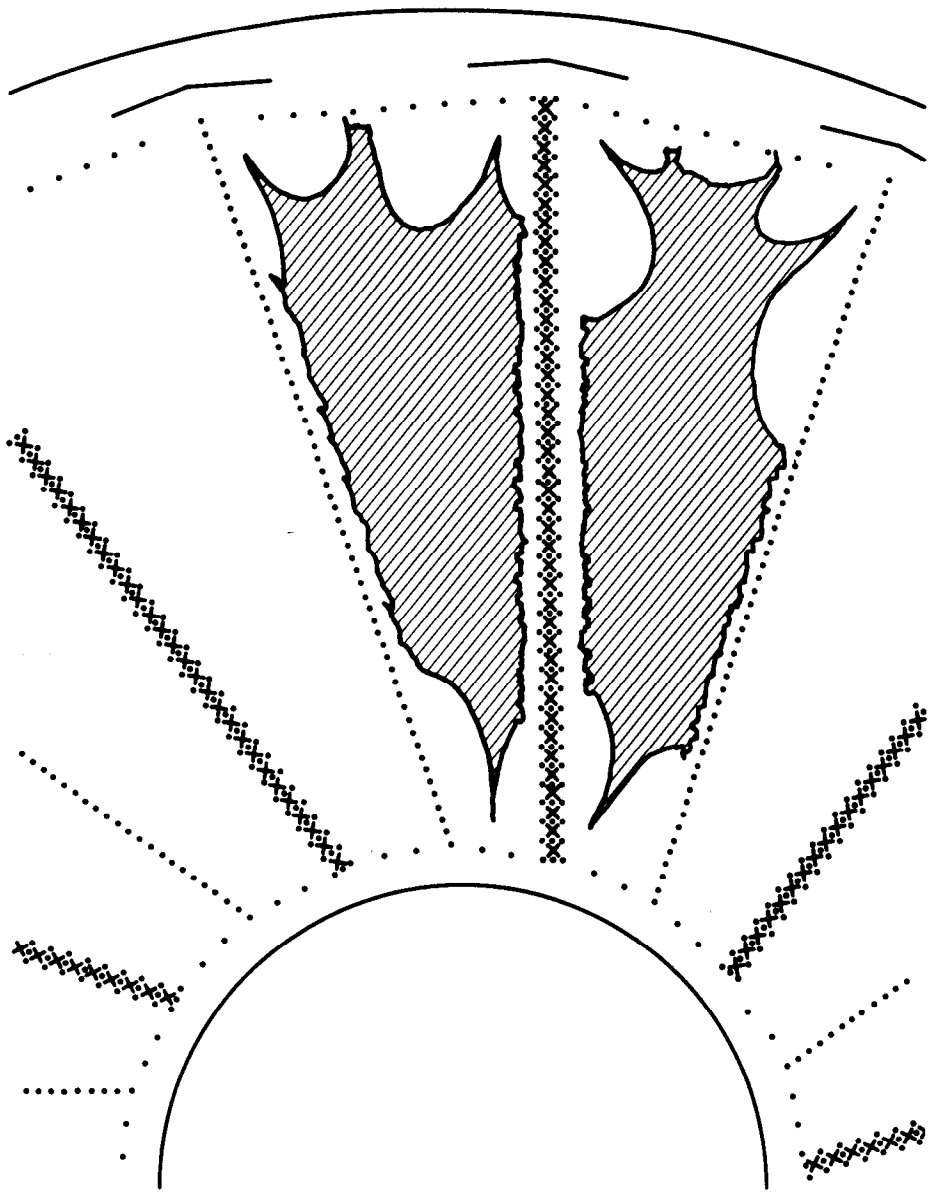

Fig. 9

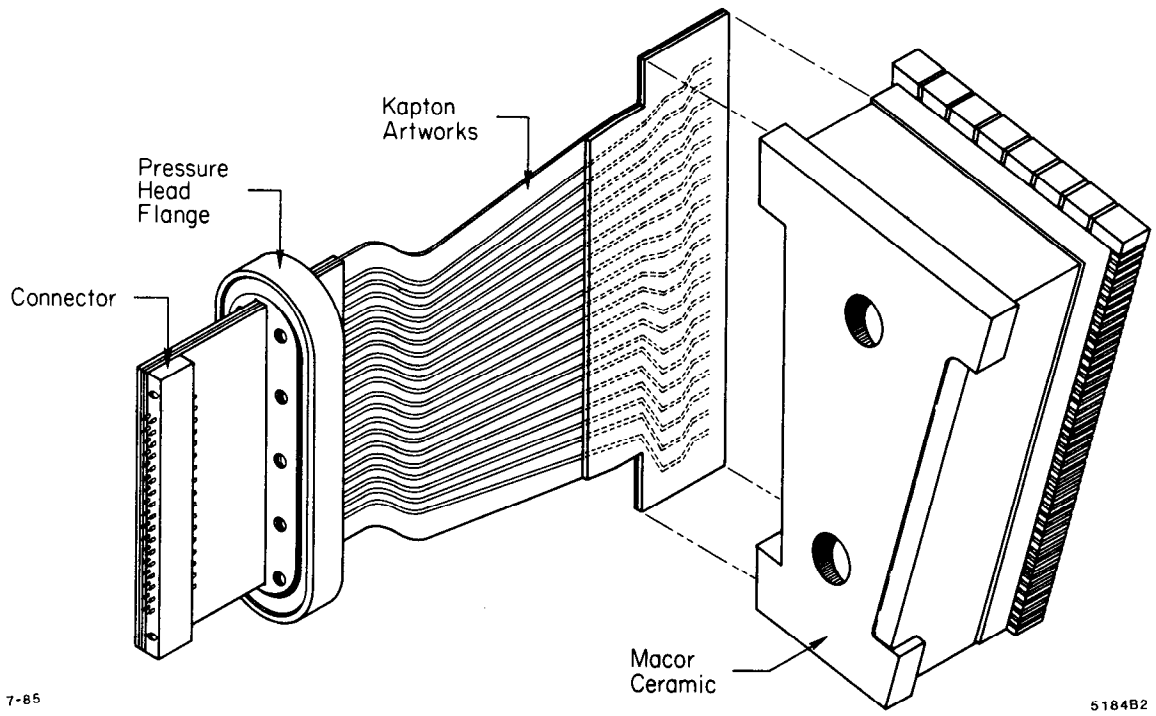
Kapton
Artworks
Pressure
Head
Flange
Connector
Macor
Ceramic
7-85
5184B2

Fig. 10